3

CIRCUMSTELLAR RADIO MOLECULAR LINES

Nguyen-Quang-Rieu

INTRODUCTION

Late-type stars radiate most of their energy in the near- and mid-infrared regions. The energy distribution of Mira variables peaks around 2 μm and the well-known infrared source, IRC + 10216, is very bright between 2 and 20 μm. Many infrared stars similar to IRC + 10216 are believed to be long-period variables, their thick circumstellar shell almost totally obscuring the central star. Reemission of stellar radiation by warm dust grains causes the infrared continuum flux. The extended shells of both visible and unidentified infrared cool stars also emit molecular emission lines at centimeter and millimeter wavelengths. Since radio lines can be excited by infrared photons, a combination of infrared and radio observations is very useful in determining molecular excitation mechanisms (Kwan and Scoville, 1974; Deguchi and Iguchi, 1976; Elitzur et al., 1976; Bujarrabal et al., 1980).

Late-type stars are characterized by mass loss (see Goldberg, this volume). Sporadic ejection of matter or modulation of a continuous process may produce stratification of the circumstellar shell (Bernat, 1981; Ridgway, 1981). As a result, molecular lines can serve to probe the physical conditions in different layers. In particular, SiO masers (rotation lines in the ground and excited vibration states) and infrared vibration/rotation molecular lines, which need extreme excitation conditions (i.e., high gas densities and temperatures), occur close to the stellar photosphere. On the other hand, millimeter thermal emission from CO and linear carbon chain molecules—the cyanopolyyne family ($HC_{2n+1}N$)—takes place in the circumstellar envelope at several 10 to 10^3 stellar radii. Different shell layers can therefore be sampled by observing appropriate molecular transitions (Figure 3-1).

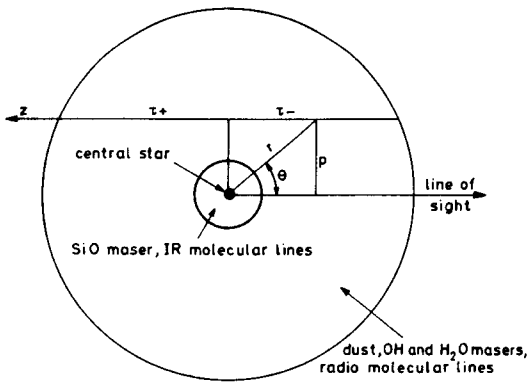

Figure 3-1. Schematic drawing of the circumstellar envelope.

CIRCUMSTELLAR MOLECULES

Molecules in space were discovered through the ultraviolet absorption lines of CH, CN, and CH^+ in stellar spectra (Swings and Rosenfeld, 1937; McKellar, 1940; Adams, 1941). The first detection of interstellar molecules at radio wavelength, the OH line at 18 cm, was made by Weinreb et al. in 1963. The improvement of radio astronomical techniques resulted later in the detection of polyatomic molecules, NH_3 and H_2O, around 1.3 cm (Cheung et al., 1968, 1969). So far, about sixty molecules and many of their isotopes have been detected, mostly in the millimeter range, in the star-forming region of Orion, in the galactic center (Sgr B2), and in the circumstellar envelope of the carbon star IRC + 10216, as well as in a number of dark clouds.

The first discoveries of circumstellar molecules were made through the detection of OH and H_2O maser lines in oxygen-rich late-type stars, mainly Mira variables and red supergiants (Wilson and Barrett, 1972; Knowles et al., 1969; Schwartz and Barrett, 1970; Robinson et al., 1971; Nguyen-Q-Rieu et al., 1971). SiO maser emission was later detected in these objects (Snyder and Buhl, 1974; Kaifu et al., 1975; Spencer et al., 1981). Subsequent systematic surveys in the 1612-MHz OH line in the galactic plane resulted in the detection of OH sources whose spectra exhibited the characteristics of OH stellar masers (Winnberg et al., 1973; Johansson et al., 1977; Bowers, 1978; Baud et al., 1979a, 1979b). These OH sources, which also have infrared but no visible counterparts (Schultz et al., 1976; Evans and Beckwith, 1977; Glass, 1978; Epchtein and Nguyen-Q-Rieu, 1982), form the so-called "unidentified OH/IR" class of objects. About 300 stars and unidentified IR objects are known to emit at least one of these maser lines (Engels, 1979).

Thermal CO emission has been detected in the envelope of carbon-rich as well as oxygen-rich stars (Solomon et al., 1971; Zuckerman et al., 1977). Other molecules containing carbon, such as HCN, HNC, and HC_3N have also been detected in some carbon-rich stars (Jewell and Synder, 1984; Olofsson et al., 1982b). In particular, 22 molecular species and their isotopes have been found in the envelope of IRC + 10216, including a complex member of the cyanopolyyne family, $HC_{11}N$, which is also the heaviest molecule so far detected in our Galaxy (Bell et al., 1982). Recently, Thaddeus et al. (1984) have identified nine of the previously unassigned lines in IRC + 10216 as those emitted by the SiC_2 radical, which turns out to be a compact symmetric ring molecule. Table 3-1 lists the circumstellar molecules. (See also Glassgold and Huggins, this volume.)

Circumstellar molecular lines are characterized by their broad line width, which reflects the large-scale expansion of the shell ($\sim$5 to 50 km s^{-1}).

MASER EMISSION

The radio emission from OH, H_2O, and SiO presents characteristics of nonthermal processes. The brightness temperature of maser sources can be as high as 10^{14} K. While OH and H_2O masers correspond to transitions in the ground vibration state $v = 0$, SiO masers occur in excited vibration states $v = 1$, 2, and 3. Recently, SiS maser emission in the ground state has also been detected in the envelope of IRC + 10216 (Henkel et al., 1983).

Masers are variable sources whose intensities are correlated with those observed in the near infrared (Hjalmarson and Olofsson, 1979). A high degree of polarization has been observed. Population inversion can be achieved through pumping by infrared radiation from warm circumstellar dust grains (Elitzur et al., 1976; Bujarrabal et al., 1980) or from the central star (Kwan and Scoville, 1974; Deguchi and Iguchi, 1976; Bujarrabal and Nguyen-Q-Rieu, 1981). Details of the pumping mechanisms will be discussed in the following sections.

Two-Level Maser

It is possible to describe a simplified maser theory by representing all details of the pumping mechanism in a two-level maser using the

Table 3-1
Molecules in Stars

Molecule	Transition	Star	Characteristics
OH	Radio	Oxygen-rich	Maser emission
H_2O	Radio	Oxygen-rich	Maser emission
SiO	Radio	Oxygen- and carbon-rich	Maser and thermal emissions
CO	Radio	Oxygen- and carbon-rich	Thermal emission
SiS	Radio	Carbon-rich	Maser and thermal emissions
CN	Radio	Carbon-rich	Thermal emission
CS	Radio	Carbon-rich	Thermal emission
HCN	Radio	Carbon-rich	Thermal emission
HNC	Radio	Carbon-rich	Thermal emission
HC_3N	Radio	Carbon-rich	Thermal emission
HC_5N	Radio	Carbon-rich	Thermal emission
HC_7N	Radio	Carbon-rich	Thermal emission
$HC_{11}N$	Radio	Carbon-rich	Thermal emission
C_2H	Radio	Carbon-rich	Thermal emission
C_4H	Radio	Carbon-rich	Thermal emission
C_3N	Radio	Carbon-rich	Thermal emission
CH_3CN	Radio	Carbon-rich	Thermal emission
SiC_2	Radio	Carbon-rich	Thermal emission
NH_3	Radio and IR	Carbon-rich	Thermal emission
C_2H_2	IR	Carbon-rich	Thermal emission
C_2H_4	IR	Carbon-rich	Thermal emission
CH_4	IR	Carbon-rich	Thermal emission

pump rates (Litvak, 1972). The populations of the upper and lower levels n_u and n_l, are given by the statistical equilibrium equation:

$$n_u (A_{ul} + B_{ul}\,\Omega I/(4\pi) + C_{ul} + P_{ul}) = n_l (B_{lu}\,\Omega I/(4\pi) + C_{lu} + P_{lu}) , \quad (3\text{-}1)$$

where A_{ul}, B_{ul} are the Einstein coefficients for spontaneous and stimulated emissions, B_{lu} is the absorption coefficient, and C_{ul} and C_{lu} are the collision rates. The pump rates, P_{ul} and P_{lu}, correspond to indirect population transfer between levels u and l through other higher levels which are not considered. P_{ul} and P_{lu} are the pump rates which transfer population to the lower and to the upper level, respectively. I is the specific intensity, and Ω is the solid angle of the microwave emission.

To simplify the explanation, we shall ignore spontaneous emission and collisions and assume that the two maser levels have the same statistical weight. The rate of fractional population inversion can then be derived from Equation (3-1):

$$\frac{n_u - n_l}{n_u + n_l} = \frac{\Delta P}{P + B_{ul}\,\Omega I/(2\pi)} , \quad (3\text{-}2)$$

where $P = P_{ul} + P_{lu}$ is the total net pump rate and $\Delta P = P_{lu} - P_{ul}$ is the difference in pump rates to the upper and lower levels.

Population inversion occurs when $\Delta P > 0$. Furthermore, the maser is saturated when the stimulated emission comes very much into evidence, $B_{ul}\,\Omega I/2\pi \gg P$. The population inversion then decreases inversely proportional to the stimulated emission rate. In the saturated

regime, the pumping is the most efficient because the population of the upper level is transferred as fast as possible to the lower level through stimulated emission. The saturation intensity is defined as:

$$I_S = 2\pi P/(B_{ul}\Omega) \quad . \tag{3-3}$$

The population inversion rate $\Delta n = n_u - n_l$ can be expressed in terms of the unsaturated rate Δn_o, which is equal to $(\Delta P/P)\ (n_u + n_l)$:

$$\Delta n = \frac{\Delta n_o}{1 + (I/I_s)} \quad . \tag{3-4}$$

The maser intensity I can be obtained by the one-dimensional radiative transfer equation:

$$\frac{dI}{dx} = -\kappa I + \epsilon \quad . \tag{3-5}$$

The absorption and emission coefficients, $\varkappa$ and ϵ, are defined as:

$$\varkappa = (n_l - n_u)\ B_{ul}\ h\nu/(4\pi\Delta\nu) \quad ,$$

$$\epsilon = n_u\ A\ h\nu/(4\pi\Delta\nu) \quad ,$$

where A is the spontaneous emission coefficient, and $h\nu$ is the level energy separation of the maser transition.

The solution of Equation (3-5) is:

$$I = I_o\, e^{-\kappa x} + \frac{\epsilon}{K}\ (1 - e^{-\kappa x}) \quad . \tag{3-6}$$

When population inversion occurs, $(n_u > n_l)$, $\varkappa$ is negative, and the maser intensity increases exponentially with path length. In the saturated regime, Equation (3-5) gives:

$$\frac{dI}{dx} \simeq \frac{\kappa_o I}{1 + (I/I_s)} \simeq -\kappa_o I_s \quad , \tag{3-7}$$

and

$$I \simeq I_s\ [1 - \varkappa_o\ (x - x_s)] \quad ,$$

where $\varkappa_o = \varkappa\ (1 + I/I_s)$ and x_s is the length where saturation begins to occur.

Equation (3-7) shows that, when the maser becomes saturated, the intensity increases linearly with path length. Litvak (1971) has shown that an unsaturated maser core can be formed at the center of a spherical saturated maser cloud.

Multilevel Radiative Transfer

A detailed study of molecular excitation requires the resolution of the radiative transfer and statistical equilibrium equations, involving many molecular levels. For an expanding spherical circumstellar cloud, the population of a level i at a distance r from the central star is given by:

$$n_i(r)\ \Sigma_j\ (A_{ij} + B_{ij}\bar{J}_{ij} + C_{ij}) = \Sigma_j\ n_j\ (r)\ (A_{ji} + B_{ij}\ \bar{J}_{ij} + C_{ji}) \quad , \tag{3-8}$$

with $A_{ij} = 0$ for $j \quad i$,

and $A_{ji} = 0$ for $j \quad i$.

A and B are the Einstein coefficients, and C represents the collision rates. The mean radiation field J, integrated over the line profile and averaged over the angle, is usually calculated by use of the escape probability formalism (see, for example, Castor, 1970):

$$\bar{J} = \left\{ 1 - \beta(r) \right\}\ S(r) + \beta_c\ (r)\ I_c \quad . \tag{3-9}$$

The source function $S(r)$ is:

$$S(r) = \frac{2h\nu^3}{c^2} \Big/ \left(\frac{n_j(r) g_i}{n_i(r) g_j} - 1 \right) , \tag{3-10}$$

where g_i and g_j are the statistical weights, β is the probability that a photon emitted at r

escapes without being absorbed by the cloud, and β_c is the probability of a photon which escapes at r and strikes the central star. In general, β_c, I_c is the contribution to the intensity of all continuum sources:

$$\beta = \int_0^1 \frac{1 - e^{-\tau(\mu)}}{\tau(\mu)} \, d\mu \quad , \qquad (3\text{-}11)$$

and

$$\beta_c \simeq \frac{\Delta\Omega}{4\pi} \left\{ \frac{1 - e^{-\tau(\mu=1)}}{\tau(\mu = 1)} \right\}, \qquad (3\text{-}12)$$

where μ is the cosine of the angle θ between a radius and the line of sight (Figure 3-2). $\Delta\Omega/4\pi$ is the dilution factor of the stellar radiation field (Bujarrabal and Nguyen-Q-Rieu, 1981).

The opacity is:

$$\tau = \frac{\tau_o}{1 + (\gamma - 1)\mu^2} \quad , \qquad (3\text{-}13)$$

where γ is the logarithmic velocity gradient $d \ln V / d \ln r$, τ_o is related to the population inversion Δn by $\tau_o \propto r\Delta n/V(r)$ (Castor, 1970), and V(r) is the expansion velocity.

The population distribution of the entire set of molecular levels can be calculated by solving Equation (3-8) and using Equations (3-9) through (3-13). In particular, the population inversion of the maser transition $i \rightarrow j$ can be determined, and hence the optical depth, as well as the excitation temperature, T_{ex}:

$$\frac{n_i}{n_j} = \frac{g_i}{g_j} \, e^{-h\nu/\kappa T_{ex}} \, . \qquad (3\text{-}14)$$

The brightness temperature of the maser source can then be calculated by an integration along the line of sight:

$$T_B = \left\{ \hat{T}_{ex} - \hat{T}_{bb} \right\} (1 - e^{-\tau}) \quad , \qquad (3\text{-}15)$$

with

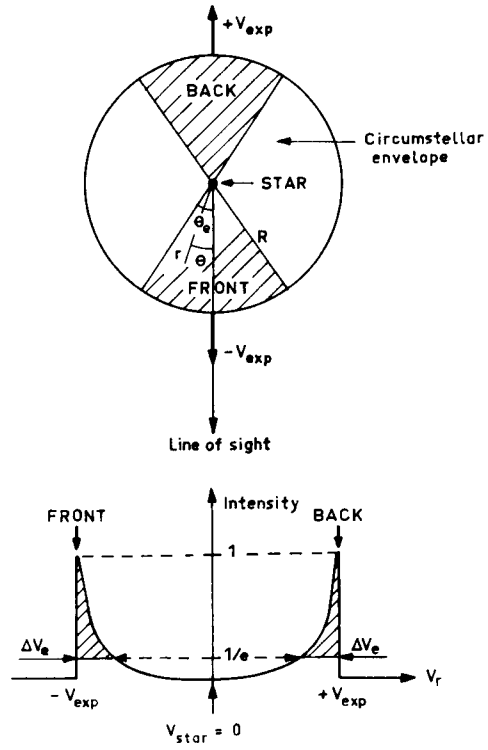

Figure 3-2. Spherical model of an OH circumstellar maser. The maser emission is confined within a double cone (hatched area) whose axis is along the line of sight (top). A schematic maser spectrum is drawn (bottom). The regions of the spectrum emanating from the hatched areas in the circumstellar envelope are also represented (hatched areas).

$$\hat{T} = \frac{h\upsilon}{k} \, (e^{h\upsilon/kT} - 1)^{-1} \quad .$$

T_{bb} is the 3 K cosmic background temperature. The convolution of T_B with the antenna beam will give the observed main-beam brightness temperature. See Equation (3-16).

Characteristics of Circumstellar Masers

Circumstellar maser emission, namely that of OH, is often characterized by a double-peaked spectrum (Figure 3-3). This shape can be explained in terms of a spherical model in which the amplification path is maximum in the direction of the line of sight which intersects

the central star (see Nguyen-Q-Rieu et al., 1979). In an expanding spherical shell for which γ is constant and positive, the velocity field can be expressed as: $V(r) = V_{exp}\,(r/R^{\gamma})$, where V_{exp} is the expansion velocity at the outer radius R. Equation (3-13) shows that the optical depth along the z axis ($\theta = 0$) is τ_0/γ (see Figure 3-1). In the case of an expansion due to radiation pressure, γ is small ($\gamma \ll 1$) and $\tau_{max} \gg \tau_0$. Hence, the maximum amplification, corresponding to the two spikes in the maser spectrum, occurs in a narrow double cone whose apex is the central star and whose axis is the line of sight (Figure 3-2). The emission at the line center corresponds to the part of the envelope outside the cone and perpendicular to the line of sight with the smallest path length. This geometrical effect is illustrated in Figure 3-2, in the case of a circumstellar shell expanding at a nearly constant velocity. The angle θ_e of the cone corresponds to the direction in which the line intensity drops to $1/e$ of the peak intensities, I_{Max}:

$$\cos\theta_e \simeq (V_{exp} - \Delta V_e)/V_{exp} \quad ,$$

where ΔV_e is the line width at $1/e\ I_{Max}$ of the narrow maser spikes.

Figure 3-3 shows the 1612-MHz OH spectrum and the maps of the maser emission from the circumstellar shell of the unidentified OH/IR object, OH26.5 + 0.6, obtained with the very large array (VLA) by Baud (1981). The maps indicate that the two maser peaks arise from two compact regions at the center of the source, while the emission toward the center of the spectrum is more extended and exhibits a ring-like structure. This observational result is consistent with the model of an expanding spherical shell described above. However, this simple model does not account for some details which can be explained by large-scale nonradial motion or turbulence which may exist in the shell.

In the framework of a symmetrical model, the OH blue-shifted and red-shifted wings correspond to the front and back of the shell, respectively. Thus, the blue-shifted wing should lead the red-shifted wing to the observer. This results in a phase lag between the blue-shifted and red-shifted components. The phase lag, which corresponds to the light travel time across the entire shell, is ~1 month for a shell size ~8 $\times$ 10^{16} cm.

The determination of the phase lag, and hence the linear source size, by means of a monitoring of the OH maser emission, combined with interferometric measurements of the angular size, constitutes a powerful method to estimate the distance of the stars (Shultz, et al., 1978; Jewell et al., 1979; Booth et al., 1981; Baud, 1981; Herman, 1983). This method has been extensively used to measure the distance of unidentified OH/IR sources for which no period/luminosity relation in the visible is available.

Another interesting feature of the OH and SiO circumstellar masers is that the maser emission is correlated with the infrared and optical phases (Harvey et al., 1974; Fillit et al., 1977; Jewell et al., 1979; Hjalmarson and Olofsson, 1979). However, the SiO fluxes appear to have a phase lag with respect to the visual light curve (see Hjalmarson and Olofsson, 1979). The correlation with the infrared fluxes suggests that the maser emission is pumped by a radiative process.

The pumping by 35-μm photons emitted by circumstellar grains may be operative in the shell and gives rise to OH masers (Elitzur et al., 1976; Bujarrabal et al., 1980). It has been suggested that direct stellar radiation can pump OH masers (Cimerman and Scoville, 1980). The pumping of the SiO and SiS masers is achieved by the infrared photons emitted by the central star. Although the OH maser emission extends far from the star, at several 10^3 stellar radii (Reid et al., 1981), SiO masers occur very close to the stellar atmosphere at a few stellar radii (Elitzur, 1980; Bujarrabal and Nguyen-Q-Rieu, 1981). This is due to the fact that OH can be excited by infrared radiation from warm circumstellar dust and that SiO is pumped by the stellar radiation. Strong SiS maser spikes also arise near the stellar surface. The pumping mechanism of H_2O masers is not well

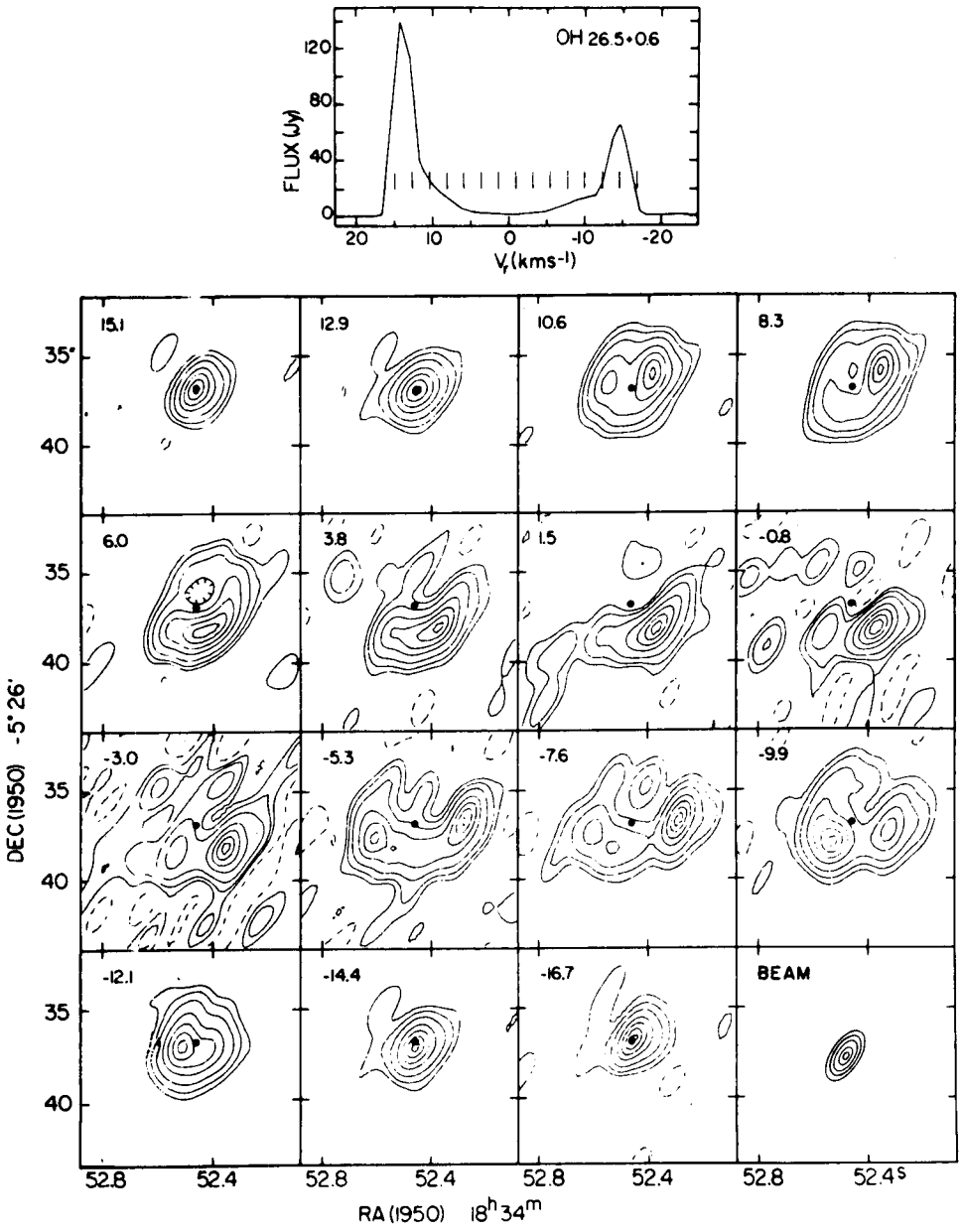

Figure 3-3. The OH spectrum (1612-MHz satellite line) (top) and the corresponding maps at different radial velocities (with respect to the stellar velocity taken equal to zero) of the OH/IR source, OH26.5 + 0.6, observed with the VLA by Baud (1981). The dot in each frame corresponds to the stellar position. Radial velocities in km s^{-1} are noted on top (left) of each frame, and the beam shape is represented in the frame at bottom right. In a spherical shell, the maps corresponding to the extreme radial velocities, 15.1 and -16.7 km s^{-1} (red-shifted and blue-shifted peaks, respectively), are associated with the part of the envelope confined within a small area in the double cone (see also Figure 3-2), where the maser amplification is maximum. The maps taken at velocities closer to the stellar velocity and corresponding to more extended areas outside the cone show a more complicated shape, in particular a ring structure (e.g., at velocities 3.8 and -5.3 km s^{-1}).

understood because of the complexity of the energy level structure.

Figure 3-4 displays the SiS maser spectrum in the ground state (v = 0, J = 1–0 at 1.65-cm wavelength of the carbon star, IRC + 10216, observed at minimum light with the 140-ft radio telescope at Green Bank together with the calculated profile (dots) derived from an excitation model of the kind described in the section *Multilevel Radiative Transfer* (Nguyen-Q-Rieu et al., 1984). The narrow maser spike at -40 km s^{-1} is likely to be produced by the amplification of the emission of the infrared core by the gas in the immediate vicinity of the core. The observations by Henkel et al. (1983) made at maximum infrared light indicate that the maser intensity is increased by ~40 percent as compared with the intensity at minimum.

The increase of the infrared flux and of the mass loss during maximum light could be responsible for the enhancement of the SiS maser emission. It is noteworthy that weak CO maser emission can exist in the circumstellar envelope (Morris, 1980).

Strong circumstellar masers are probably saturated. They are usually not subject to erratic time variation, but instead vary smoothly with the stellar phase.

OH emission is known to be polarized, up to ~60 percent (Robinson et al., 1970). Circular polarization is usually observed, but in some cases, polarization can change from circular to linear. Significant linear polarization has been detected in SiO maser spectra (Troland et al., 1979). The position angles of the polarized features vary with time. In the case of the Mira variable, R Cas, sudden changes in the position angles have been detected near the maximum of the optical light curve (Clark et al., 1982). Shock waves which can affect the gain paths and the orientation of the maser cells are believed to be responsible for this sudden variation.

THERMAL EMISSION

Thermal CO emission in the ground-state (v = 0, J = 1–0) at 2.6 mm has been discovered

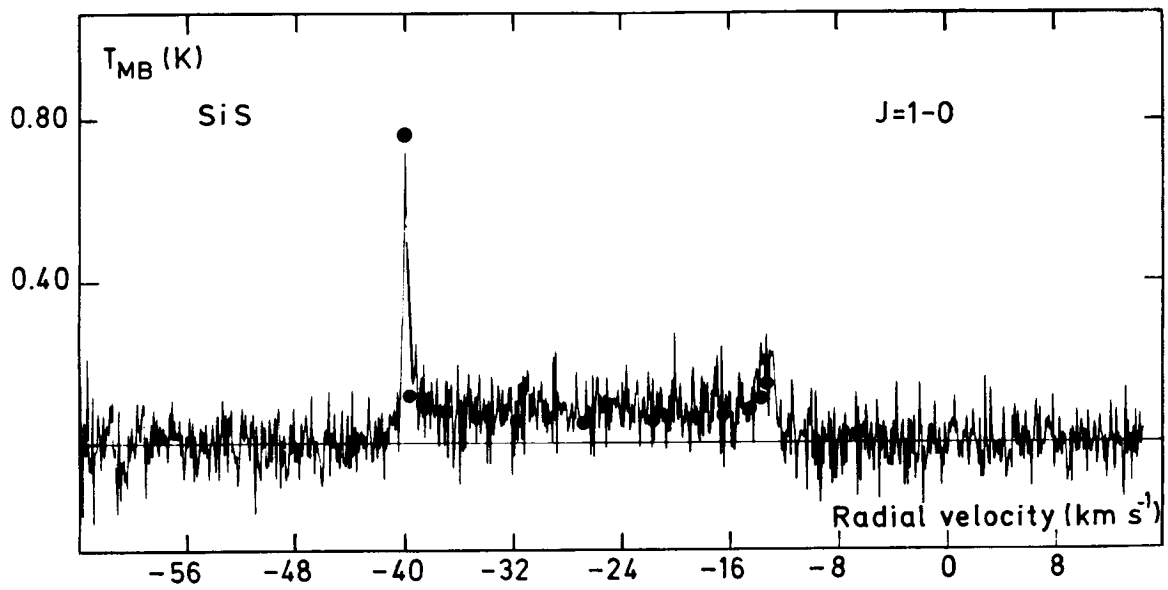

Figure 3-4. The 18155-MHz SiS (J = 1–0) spectrum of the carbon star IRC + 10216. Dots correspond to the theoretical spectrum derived from an excitation model. The blue-shifted feature at -40 km s^{-1} is the result of an amplification of the background stellar core by the SiS circumstellar maser cloud (from Nguyen-Q-Rieu et al., 1984).

in the envelope of the carbon star, IRC + 10216 (Solomon et al., 1971). Thermal emission from SiO, CO, CN, and CS (ground-state) and their isotopes was later detected in a number of oxygen-rich and carbon-rich stars, as well as in some S-type stars (Wilson et al., 1971; Zuckerman et al., 1977, 1978; Lo and Bechis, 1977; Lambert and Vanden Bout, 1978; Wannier et al., 1979; Olofsson et al., 1982a). Molecular species like HNC, HCN, HC_3N, and other linear carbon chain molecules also exist in the shell of carbon-rich stars (Jewell and Snyder, 1984; Olofsson et al., 1982b).

Figure 3-5 shows the spectra of HNC (J = 1-0), SiS (J = 5-4), and HC_3N (J = 10-9) observed simultaneously in the direction of IRC + 10216 using the millimeter Onsala radiotelescope equipped with a broadband receiver (Olofsson et al., 1982a).

Contrary to SiO masers which arise in the vicinity of the central star, thermal molecular line emission extends over the entire envelope. In this respect, thermal spectra give information on the physical parameters of the entire shell (namely, the mass loss, gas, and dust densities). For example, spatial CO mapping of the envelope of IRC + 10216 suggests that the present mass loss rate may have been higher in the past (Wannier et al., 1979). The determination of the abundance of molecules and their isotopic substitutes is useful in the understanding of the processing of matter involving the mixing mechanisms (Iben, 1981) and the photodestruction process caused by the interstellar ultraviolet radiation field (Huggins and Glassgold, 1982). Neutral/neutral reactions seem to be important in circumstellar shells, while interstellar chemistry is dominated by ion/molecule reactions. This is due to the fact that high temperatures (>100 K) allow endothermic reactions, as well as others with activation energy barriers, to proceed in the circumstellar envelope (Scalo and Slavsky, 1980; Lafont et al., 1982).

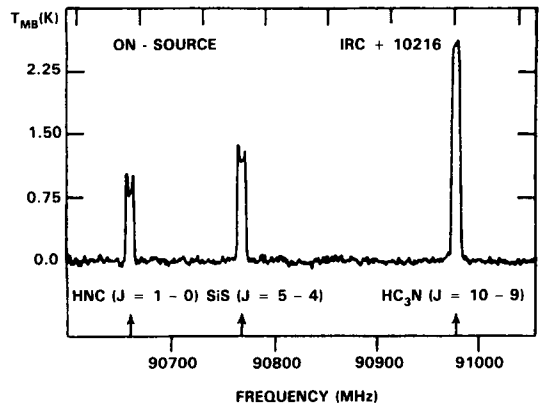

Figure 3-5. Simultaneous observations of HNC, SiS, and HC_3N lines around 91000 MHz from IRC + 10216, using a broadband receiver installed at the focus of the 20-m Onsala radio telescope (from Olofsson et al., 1982a).

Molecular Excitation and Line Profiles

The excitation of circumstellar molecules is governed by Equation (3-8) in which both collisional and radiative processes are involved. Collisions, essentially with H_2, tend to thermalize the lines. This is usually the case with CO lines in dense envelopes. Infrared radiation from the central star and dust embedded in the envelope can produce population inversion as discussed in the section *Characteristics of Circumstellar Masers.*

The main-beam brightness temperature, T_{MB}, at a radial velocity, V_r, is obtained by convolving the brightness temperature distribution, T_B (see Equation (3-15)) with the antenna main beam, which is assumed to be gaussian (Olofsson et al., 1982a):

$$T_{MB}(V) = \frac{81n2}{B^2} \int_{pmin}^{pmax} T_B(p, V_r)\, e^{-41n2\,(p/B)^2}\, pdp \quad , \tag{3-16}$$

where B is the full width at half power (FWHP) of the antenna beam and $p = r\left\{1 - (V_r/V_{exp})^2\right\}^{1/2}$ (see Figure 3-1). In Equation (3-16), we have assumed a uniformly excited

spherical shell (T_{ex} is constant throughout the shell), expanding at a constant velocity. If the mass-loss rate is constant, the total particle density is $N(r) \propto r^{-2}$. The optical depth can be expressed as (Olofsson et al., 1982a):

$$\tau(p,V_r) = \tau(B,0) \times B \left\{ p\,(1 - V_r/V_{exp})^2)^{1/2} \right\}^{-1} .$$

The diagram (Figure 3-6) which represents the line profiles T_{MB} (V_r) as a function of the optical depth, τ(B,0), and the shell size, R_e, expressed in units of beamwidth, B, is calculated using Equation (3-16).

For an unresolved optically thin shell (position 1 in the diagram), the profile is rectangular. The line shape is parabolic if the shell is optically thick (position 2) and becomes flatter when the shell size is extended with respect to the antenna beam (positions 3 and 5). The profile can exhibit a double-peaked structure for an optically thin and resolved shell (position 4). These effects can be explained by the fact that, when the source is resolved by the telescope beam, the part of the shell which is not inside the beam corresponds to low radial velocity line center. As a result, the contribution of this outer shell to the main-beam brightness temperature is not important and leads to a more or less pronounced depression at the line center. Therefore, a quick inspection of the line profiles can indicate the nature of the circumstellar shell.

Line Asymmetry and Time Variation

Figure 3-7 shows a variety of line profiles observed in the direction of IRC + 10216

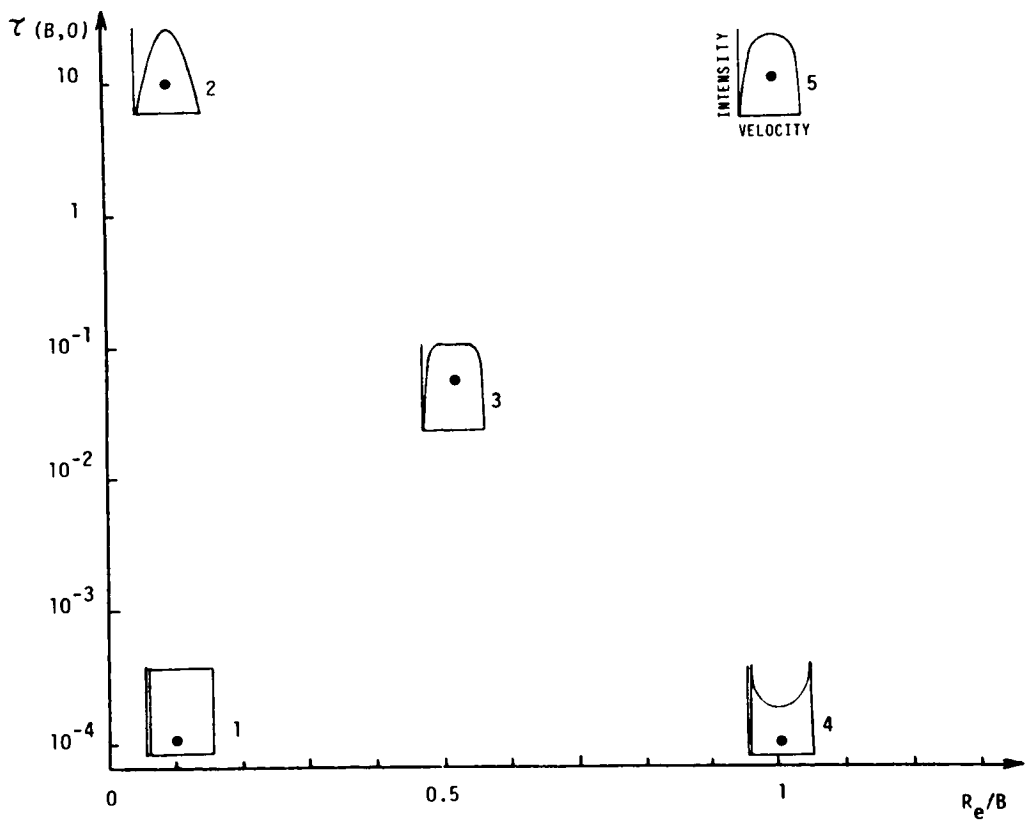

Figure 3-6. A diagram representing various line shapes as a function of optical depth (ordinate) and source size R_e in unit of beamwidth B (abscissa). Dots correspond to the points in the diagram for which the line profiles are calculated.

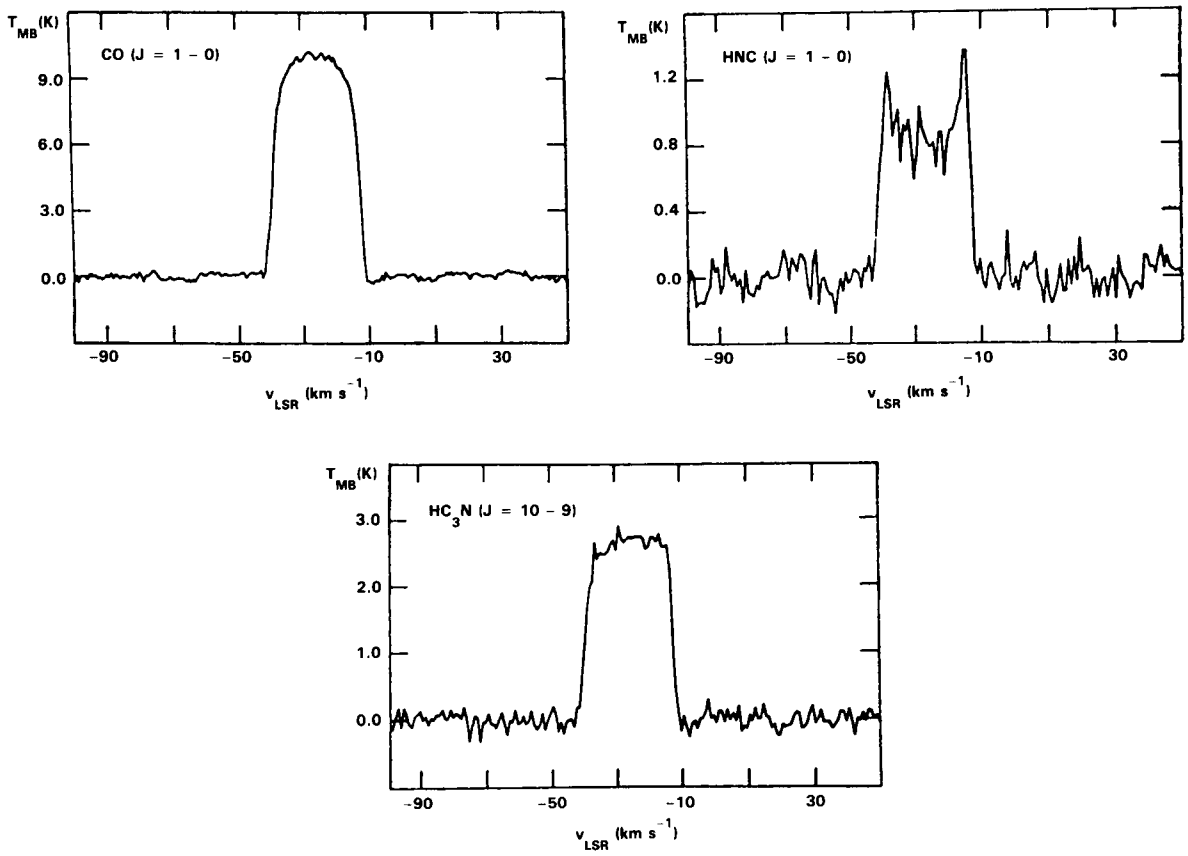

Figure 3-7. A sample of spectra (CO at 115271 MHz, HNC at 90663 MHz, and HC_3N at 90979 MHz) from IRC + 10216 obtained with a high resolution spectrometer $\nu/\Delta\nu \sim 4 \times 10^5$) (from Olofsson et al., 1982a). V_{LSR} is the radial velocity relative to the local standard of rest.

(Olofsson et al., 1982a). The spectra correspond to different line opacities and source sizes, according to the diagram shown in Figure 3-6. The CO line emanates from an optically thick extended shell. The HNC and HC_3N transitions correspond to optically thin regions. Although the HNC shell is resolved by the telescope beam, the HC_3N shell appears to be a point source. Theoretically, an estimate of the shell parameters can be derived by fitting the main-beam brightness temperature profiles, calculated by using Equation (3-16), to the observed spectra. However, the observed profiles (Figure 3-7) present some asymmetry in the sense that the blue-shifted wing is systematically weaker than the red-shifted one. This effect is most prominent in the case of ^{13}CO (Figure 3-8). It should be mentioned that in the SiS J = 1-0 profile (Figure 3-4), the depression of the blue-shifted wing is disguised by the maser action which amplifies the stellar radiation and thereby gives rise to a narrow spike at the blue wing.

In fact, the hypothesis of a constant excitation temperature throughout the circumstellar cloud cannot account for the line asymmetry. The inner shell is more excited and hotter than the outer shell. As a result, along the line of sight, outer colder material is absorbing emission from the hotter inner layers in the front hemisphere, but such absorption does not affect the back hemisphere. Similar asymmetry also seems to be observed in α Ori (Knapp et al., 1980).

In order to account for this effect, instead of using Equation (3-15), we shall calculate the

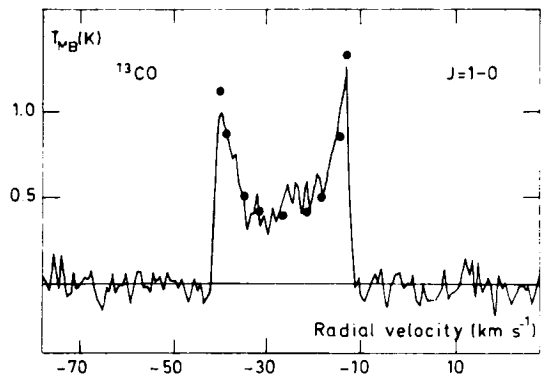

Figure 3-8. The ^{13}CO spectrum (110201 MHz) from IRC + 10216 showing the line asymmetry (blue-shifted wing weaker than red-shifted wing). Dots represent the spectrum derived from a theoretical model (Nguyen-Q-Rieu et al., 1984) which explains the asymmetry in terms of an absorption of the emission from the hot inner part of the envelope by the colder outer layers.

brightness temperature separately for the front (T_{B-}) and back (T_{B+}) hemispheres by integrating along the line of sight (see Figure 3-1):

$$T_{B-} = \int_{-\infty}^{0} (\hat{T}_{ex}(z) - \hat{T}_{bb})\, e^{-\tau_-(z)}\, \kappa(z) dz \quad . \tag{3-17}$$

$$T_{B+} = \int_{0}^{\infty} (\hat{T}_{ex}(z) - \hat{T}_{bb})\, e^{-\tau_+(z)}\, \kappa(z)\, dz \quad . \tag{3-18}$$

With

$$\tau_- = \int_{-\infty}^{z} \kappa(z')\, dz'$$

and

$$\tau_+ = \int_{0}^{z} \kappa(z')\, dz' ,$$

$\kappa(z)$ is the line absorption coefficient.

Figure 3-8 displays the observed ^{13}CO spectrum of IRC + 10216, together with the spectrum computed (dots) by Equations (3-17), (3-18), and (3-16) (Nguyen-Q-Rieu et al., 1984; see also Morris et al., 1985).

The molecular line shape is sensitive to the variation of infrared light. At the maximum of the infrared light curve, infrared photons (~ 10 μm) escaping from the central heating sources (star or infrared core) can affect the outer shell and enhance the line wings (Sahai et al., 1984). The contrast between the line wings and the line center can be higher at maximum light than at minimum. In the case of IRC + 10216, it has been shown that, at maximum, the line center and the line wings of the SiS $J = 6$–5 transition can be enhanced by ~ 20 and ~ 40 percent, respectively (Nguyen-Q-Rieu et al., 1984).

CONCLUSION AND PROSPECTS

Radio molecular lines appear to be useful probes into the stellar environment. SiO masers which are excited by stellar photons to a vibrational level as high as $v = 3$ (Scalise and Lépine, 1978), which corresponds to an energy $E/k \sim 5300$ K, provide information on the physical conditions in the immediate vicinity of the stellar photosphere. Lower vibrationally excited transitions of SiO occur in $v = 0$ and 1 ($E/k \lesssim 1800$ K) sample regions in which dust grains begin to form. The proximity of SiO masers to the pulsating stellar atmosphere implies that SiO observations can shed light on the kinematics and mass-loss process in the innermost layers. As explained in the sections *Multilevel Radiative Transfer* and *Characteristics of Circumstellar Masers*, the maser amplification and hence the line shape depend on the velocity gradient. SiO maser emission does not usually exhibit a double-peaked profile typical of OH masers, but a single feature centered at the stellar velocity. This observational difference

suggests that the velocity gradient in the inner region in which SiO occurs is higher (see Equation (3-13), where $\gamma = d\log V/d\log r$ is now $>> 1$) than in the external envelope in which OH masers are located ($\gamma << 1$). OH masers and thermal molecular emission of CO and other molecules, including cyanopolyynes, which can be excited by collisions with H_2 and by infrared radiation from circumstellar dust, can be used as probes into the physical conditions (on a larger scale) throughout the envelope. Valuable information on the physics operating in the envelope of IRC + 10216 has been recently obtained by high sensitivity observations and detailed theoretical analyses (Morris, 1975; Wannier et al., 1979; Kwan and Linke, 1982; Olofsson, et al., 1982a; Nguyen-Q-Rieu et al., 1984). However, accurate circumstellar chemistry still suffers from the lack of data on chemical processes. Chemistry is usually assumed to be frozen at its equilibrium state in the inner region and unchanging during the expansion of the envelope (McCabe et al., 1979). This is probably true for species which are not highly reactive, but not for radicals. Nonequilibrium chemistry may take place, for instance, in the regions in which molecular abundances are governed by photodissociation, which tends to produce radicals (Goldreich and Scoville, 1976; Scalo and Slavsky, 1980; Lafont et al., 1982). In this respect, mapping of the envelope of IRC + 10216 in the molecular lines emitted by some radicals and parent molecules is highly desirable. Present molecular observations of the envelopes of stars of various types (Olofsson et al., 1982b) and those with the millimeter radio telescopes of Institut de Radioastronomie Millimétrique (IRAM) may also cast some light on the problem of chemistry (see Glassgold and Huggins, this volume).

Infrared speckle interferometry in the molecular lines (Dyck et al., 1983) and in the continuum (Foy et al., 1979; Dyck et al., 1984) is helpful in the investigation of the inner region of the envelope.

The distribution of the circumstellar dust, whose emission contributes to the molecular excitation, can be determined by photometric measurements with a range of 1 to ~ 100 μm. In this respect, the preliminary results obtained with the instruments on board the Infrared Astronomical Satellite (IRAS) seem to indicate that many infrared objects associated with OH masers are extremely red and may experience mass-loss rates higher than 10^{-4} $M_\odot$ yr^{-1} (Olnon et al., 1984). High resolution spectroscopy using the Infrared Space Observatory (ISO) will also be of great importance in the detection of molecular transitions in a wide range of infrared wavelengths.

REFERENCES

Adams, W.S. 1941, *Astrophys. J.*, **93**, 11.

Baud, B. 1981, *Astrophys. J. (Letters)*, **250**, L79.

Baud, B., Habing, H.J., Matthews, H.E., and Winnberg, A. 1979a, *Astron. Astrophys. Supplement*, **35**, 179.

Baud, B., Habing, H.J., Matthews, H.E., and Winnberg, A. 1979b, *Astron. Astrophys. Supplement*, **36**, 193.

Bell, M.B., Feldman, P.A., Kwok, S., and Matthews, H.E. 1982, *Nature*, **295**, 389.

Bernat, A.P. 1981, *Astrophys. J.*, **246**, 184.

Booth, R.S., Kus, A.J., Norris, R.P., and Porter, N.D. 1981, *Nature*, **290**, 382.

Bowers, P.F. 1978, *Astron. Astrophys. Supplement*, **31**, 127.

Bujarrabal, V., Guibert, J., Nguyen-Q-Rieu, and Omont, A. 1980, *Astron. Astrophys.*, **84**, 311.

Bujarrabal, V., and Nguyen-Q-Rieu 1981, *Astron. Astrophys.*, **102**, 65.

Castor, J.I. 1970, *Mon. Not. Roy. Astr. Soc.*, **149**, 111.

Cheung, A.C., Rank, D.M., Townes, C.H., Thornton, D.D., and Welch, W.J. 1968, *Phys. Rev. Letters*, **21**, 1701.

Cheung, A.C., Rank, D.M., Townes, C.H., and Welch, W.J. 1969, *Nature*, **221**, 917.

Cimerman, M., and Scoville, N. 1980, *Astrophys. J.*, **239**, 526.

Clark, F.O., Troland, T.H., and Johnson, D.R. 1982, *Astrophys. J.*, **261**, 569.

Deguchi, S., and Iguchi, I. 1976, P.A.S.J. **28**, 307.

Dyck, H.M., Beckwith, S., and Zuckerman, B. 1983, *Astrophys. J. (Letters)*, **271** , L79.

Dyck, H.M., Zuckerman, B., Leinert, C., and Beckwith, S. 1984, *Astrophys. J.*, **287**, 801.

Elitzur, M. 1980, *Astrophys. J.*, **240**, 553.

Elitzur, M., Goldreich, P., and Scoville, N. 1976, *Astrophys. J.*, **205**, 384.

Engels, D. 1979, *Astron. Astrophys. Supplement*, **36**, 337.

Epchtein, N., and Nguyen-Q-Rieu 1982, *Astron. Astrophys.*, **107**, 229.

Evans, N.J., and Beckwith, S. 1977, *Astrophys. J.*, **217**, 729.

Fillit, R., Proust, D., and Lépine, J.R.D. 1977, *Astron. Astrophys.*, **58**, 281.

Foy, R., Chelli, A., Sibille, F., and Léna, P. 1979, *Astron. Astrophys.*, **79**, L5.

Glass, I.S. 1978, *Mon. Not. Roy. Astr. Soc.*, **182**, 93.

Goldreich, P., and Scoville, N.Z. 1976 *Astrophys. J.*, **205**, 144.

Harvey, P.M., Bechis, K.P., Wilson, W.J., and Ball, J.A. 1974, *Astrophys. J. Supplement*, **27**, 331.

Henkel, C., Matthews, H.E., and Morris, M. 1983, *Astrophys. J.*, **267**, 184.

Herman, J. 1983, Thesis, Sterrewacht Leiden.

Hjalmarson, A., and Olofsson, H. 1979, *Astrophys. J. (Letters)*, **234**, L199.

Huggins, P.J., and Glassgold, A.E. 1982, *Astron. J.*, **87**, 1828.

Iben, I., Jr. 1981, in *Physical Processes in Red Giants*, ed. I. Iben, Jr., and A. Renzini, (Dordrecht: Reidel), p. 3.

Jewell, P.R., Elitzur, M., Webber, J.C., and Snyder, L.E. 1979, *Astrophys. J. Supplement*, **41**, 191.

Jewell, P.R., and Snyder, L.E. 1984, *Astrophys. J.*, **278**, 176.

Johansson, L.E.B., Andersson, C., Goss, W.M., and Winnberg, A. 1977, *Astron. Astrophys. Supplement*, **28**, 199.

Kaifu, N., Buhl, D., and Snyder, L.E. 1975, *Astrophys. J.*, **195**, 359.

Knapp, G.R., Phillips, T.G., and Huggins, P.J. 1980, *Astrophys. J. (Letters)*, **242**, L25.

Kwan, J., and Linke, R.A. 1982, *Astrophys. J.*, **254**, 587.

Kwan, J., and Scoville, N. 1974, *Astrophys. J. (Letters)*, **194**, L97.

Knowles, S.H., Mayer, C.H., Cheung, A.C., Rank, D.M., and Townes, C.H. 1969, *Science*, **163**, 1055.

Lafont, S., Lucas, R., and Omont, A. 1982, *Astron. Astrophys.*, **106**, 201.

Lambert, D.L., and Van den Bout, P.A. 1978, *Astrophys. J.*, **221**, 854.

Litvak, M.M. 1971, *Astrophys. J.*, **170**, 71.

Litvak, M.M. 1972, *Collisional and Radiative Processes in Interstellar Molecules*, Part I, ed. A. Sume, Research Lab. of Electronics and Onsala Space Observatory.

Lo, K.Y., and Bechis, K. 1977, *Astrophys. J. (Letters)*, **281**, L27.

McCabe, E.M., Smith, R.C., and Clegg, R.E.S. 1979, *Nature*, **281**, 263.

McKellar, A. 1940, P.A.S.P. **52**, 187.

Morris, M. 1975, *Astrophys. J.*, **197**, 603.

Morris, M. 1980, *Astrophys. J.*, **236**, 823.

Morris, M., Lucas, R., and Omont, A. 1985, *Astron. Astrophys.*, **142**. 107.

Nguyen-Q-Rieu, Bujarrabal, V., Olofsson, H., Johansson, L.E.B., and Turner, B.E. 1984, *Astrophys. J.*, **286**, 276.

Nguyen-Q-Rieu, Fillit, R., and Gheudin, M. 1971, *Astron. Astrophys.*, **14**, 154.

Nguyen-Q-Rieu, Laury-Micoulaut, C., Winnberg, A., and Schultz, G.V. 1979, *Astron. Astrophys.*, **75**, 351.

Olnon, F.M., Baud, B., Habing, H., de Jong, T., Harris, S., and Pottasch, S.R. 1984, *Astrophys. J. (Letters)*, **278**, L41.

Olofsson, H., Johansson, L.E.B., Hjalmarson, A., and Nguyen-Q-Rieu. 1982a, *Astron. Astrophys.*, **107**, 128.

Olofsson, H., Johansson, L.E.B., Nguyen-Q-Rieu, Sopka, R.J., and Zuckerman, B. 1982b, Bull. Amer. Astron. Soc., **14**, 895.

Reid, M.J., Moran, J.M., and Johnston, K.J. 1981, *Astron. J.*, **86**, 897.

Ridgway, S.T. 1981, in *Physical Processes in Red Giants*, ed. I. Iben, Jr., and A. Renzini (Dordrecht: Reidel), p. 305.

Robinson, B.J., Caswell, J.L., and Goss, W.M. 1970, *Astrophys. Letters*, **7**, 79.

Robinson, B.J., Caswell, J.L., and Goss, W.M. 1971, *Astrophys. Letters*, **7**, 163.

Sahai, R., Wootten, A., and Clegg, R.E.S. 1984, *Astrophys. J.*, **284**, 144.

Scalise, E., and Lépine, J.R.D. 1978, *Astron. Astrophys.*, **65**, L7.

Scalo, J.M., and Slavsky, D.B. 1980, *Astrophys. J. (Letters)*, **239**, L73.

Schultz, G.V., Kreysa, E., and Sherwood, W.A. 1976, *Astron. Astrophys.*, **50**, 171.

Schultz, G.V., Sherwood, W.A., and Winnberg, A. 1978, *Astron. Astrophys.*, **63**, L5.

Schwartz, P.R., and Barrett, A.H. 1970, *Astrophys. J. (Letters)*, **159**, L123.

Snyder, L.E., and Buhl, D. 1974, *Astrophys. J. (Letters)*, **189**, L31.

Solomon, P., Jefferts, K.B., Penzias, A.A., and Wilson, R.W. 1971, *Astrophys. J. (Letters)*, **163**, L53.

Spencer, J.H., Winnberg, A., Olnon, F.M., Schwartz, P.R., Matthews, H.E., and Downes, D. 1981, *Astron. J.*, **86**, 392.

Swings, P., and Rosenfeld, L. 1937, *Astrophys. J.*, **86**, 483.

Thaddeus, P., Cummins, S.E., and Linke, R.A. 1984, *Astrophys. J. (Letters)*, **283**, L45.

Troland, T.H., Heiles, C., Johnson, D.R., and Clark, F.O. 1979, *Astrophys. J.*, **232**, 143.

Wannier, P.G., Leighton, R.B., Knapp, G.R., Redman, R.O., Phillips, T.G., and Huggins, P.J. 1979, *Astrophys. J.*, **230**, 149.

Wilson, R.W., Solomon, P.M., Penzias, A.A., and Jefferts, K.B. 1971, *Astrophys. J. (Letters)*, **169**, L35.

Wilson, W.J., and Barrett, A.H. 1972, *Astron. Astrophys*, **17**, 385.

Winnberg, A., Goss, W.M., Hoglund, B., and Johansson, L.E.B. 1973, *Astrophys. Letters*, **13**, 125.

Zuckerman, B., Palmer, P., Gilra, D.P., Turner, B.E., and Morris, M. 1978, *Astrophys. J. (Letters)*, **220**, L53.

Zuckerman, B., Palmer, P., Morris, M., Turner, B.E., Gilra, D.P., Bowers, P.F., and Gilmore, W. 1977, *Astrophys. J. (Letters)*, **211**, L97.